SUPPLEMENTARY INFORMATION

Morisaki et al. Single Molecule Analysis of TF binding

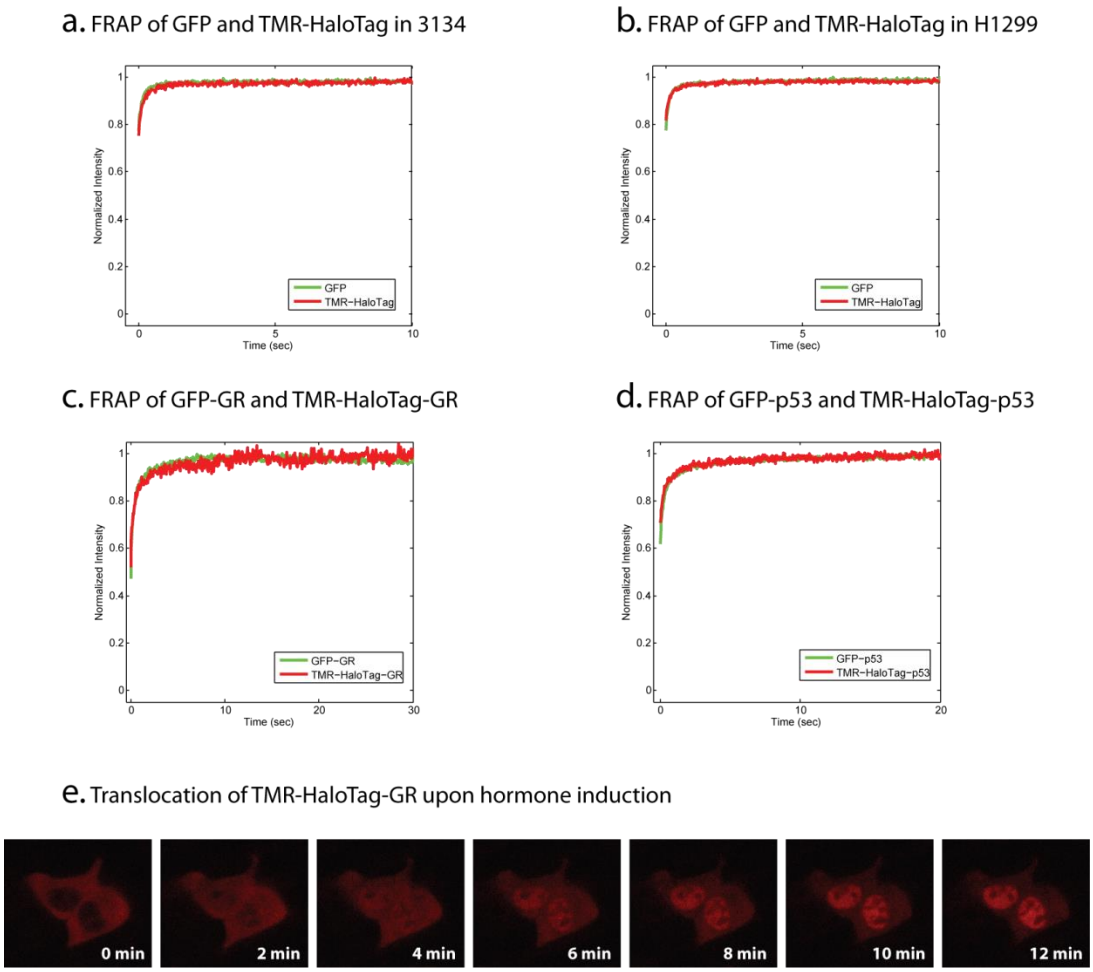

Supplementary Figure 1: Controls for the HaloTag. To test if the HaloTag itself might interact with chromatin or other nuclear constituents, we performed FRAP of the unconjugated HaloTag and compared it to FRAP of unconjugated GFP. We found that the HaloTag by itself and GFP alone gave similar FRAP recoveries in the two cell lines used in the current study, mouse adenocarcinoma 3134 cells (a) and human H1299 cells (b). This indicates that the HaloTag does not interact with nuclear components in either of these two cell lines. To evaluate the effect of the HaloTag on the binding dynamics of TFs, we performed FRAP of HaloTag GR and HaloTag p53. The FRAP curves for the HaloTag versions closely resembled the FRAP curves for the commonly used GFP tagged versions for both GR (c) and p53 (d). This indicates that both TFs exhibit similar nuclear dynamics regardless of the fusion protein tag. As a second test of the mobility of the GR HaloTag fusion, we evaluated import of HaloTag-GR into the cell nucleus following hormone addition. Shown are two cells imaged as a function of time after hormone addition at t=0 min (e). GR import occurs in ~10 min consistent with previous measurements using GFP-GR (see Supplementary Fig. 2 in [1])

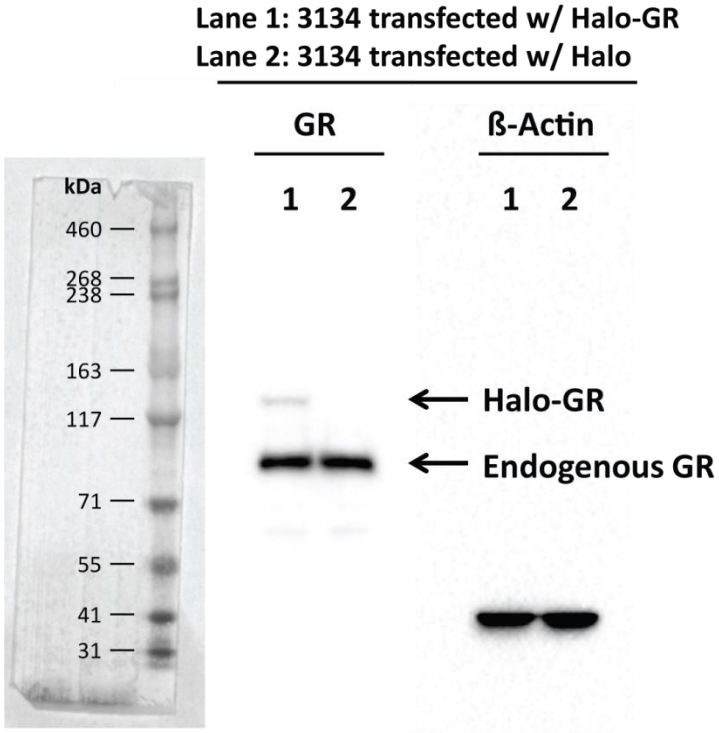

Supplementary Figure 2: Comparison of expression level between Halo-GR and endogenous GR. For GR experiments, we used the 3134 cell line because it allows us to study binding of GR to the tandem array of MMTV reporters and compare that to binding in the rest of the nucleus. In order to evaluate the relative expression level of the HaloTag GR fusion to the endogenous GR, we performed westerns in 3134 cells. We found that the Halo-GR (123 kDa) is significantly underexpressed compared to the endogenous GR (87.5 kDa). This indicates that the small bound fractions we measured were not due to overexpression of exogenous GR molecules. Note that we confirmed that almost all cells were transiently transfected with Halo-GR by checking the fluorescence from a co-transfected GFP-polymerase II.

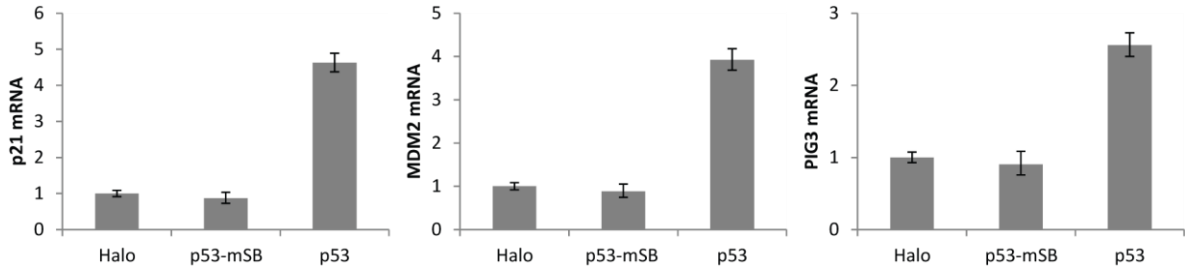

Supplementary Figure 3: qPCR for mRNA expression from H1299 cells expressing HaloTag fussed p53 and mutant (p53-mSB). We performed RT-PCR of mRNA of p53 target genes (p21, MDM2 and PIG3) and found induction of expression by p53-Halo, but not by p53-mSB-Halo. These results suggest that p53-Halo can activate target genes without stress, and that p53-mSB-Halo cannot activate target genes (n = 3, error bars represent the s.d.).

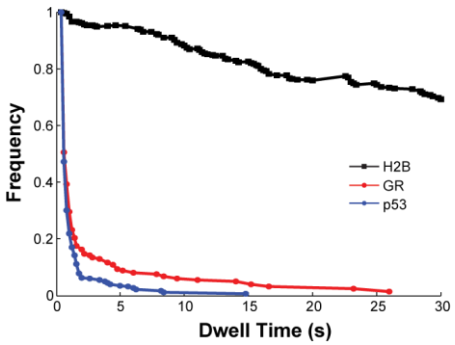

Supplementary Figure 4: H2B cumulative histogram. Dwell times of H2B in 3134 cells were measured and plotted using the same procedure as described for the two TFs. Note that the H2B histogram decays on a much slower time scale suggesting that longer residence times could be measured under our conditions, and that the decays seen for GR and p53 are not significantly limited by photobleaching.

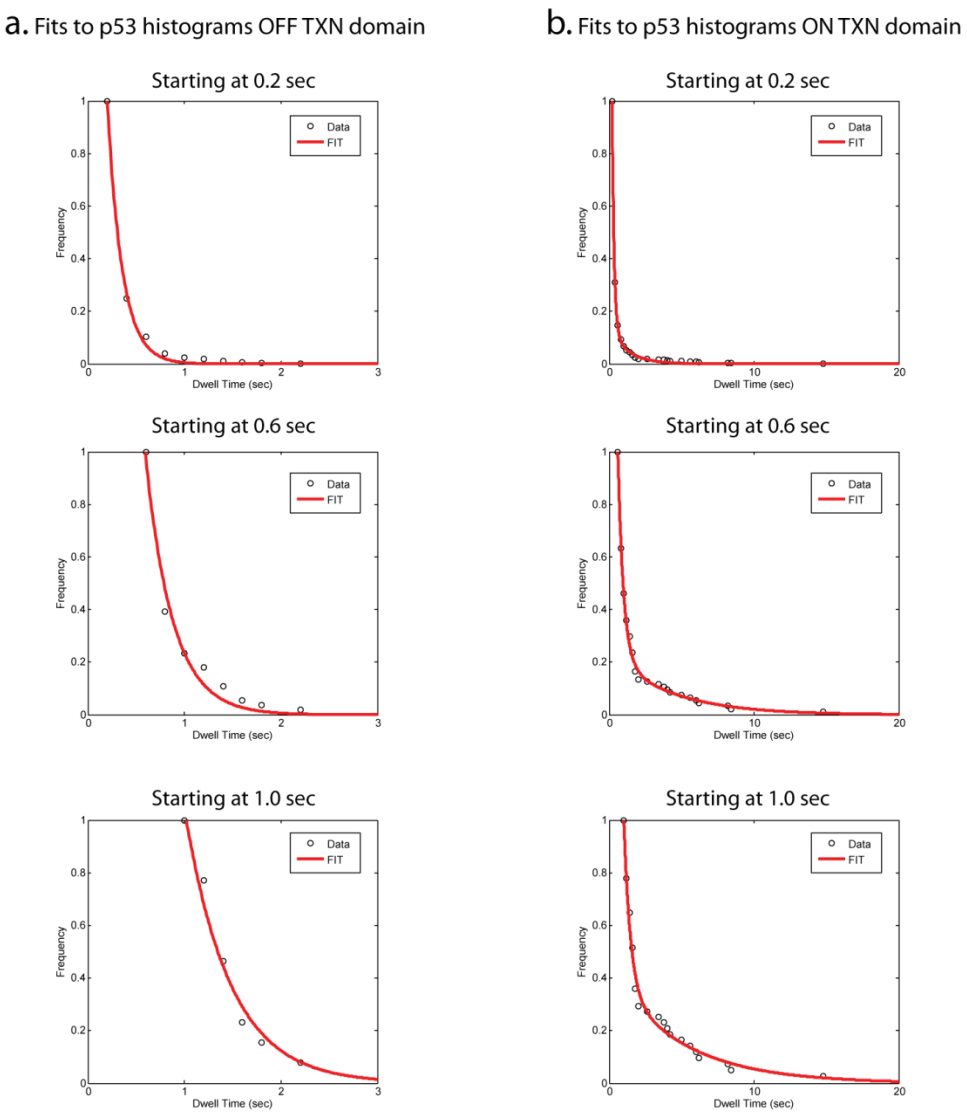

Supplementary Figure 5: Fits to the cumulative histograms. The cumulative histograms away from transcription domains were fit with a single exponential decay (left panels), while the cumulative histograms at transcription domains were fit with a double exponential decay (right panels). Fits are shown for cases using all the data (upper 2 panels), or dropping the first 2 data points (middle 2 panels), or dropping the first 4 data points (bottom 2 panels). In all cases, we could obtain good fits with the exponential decay models.

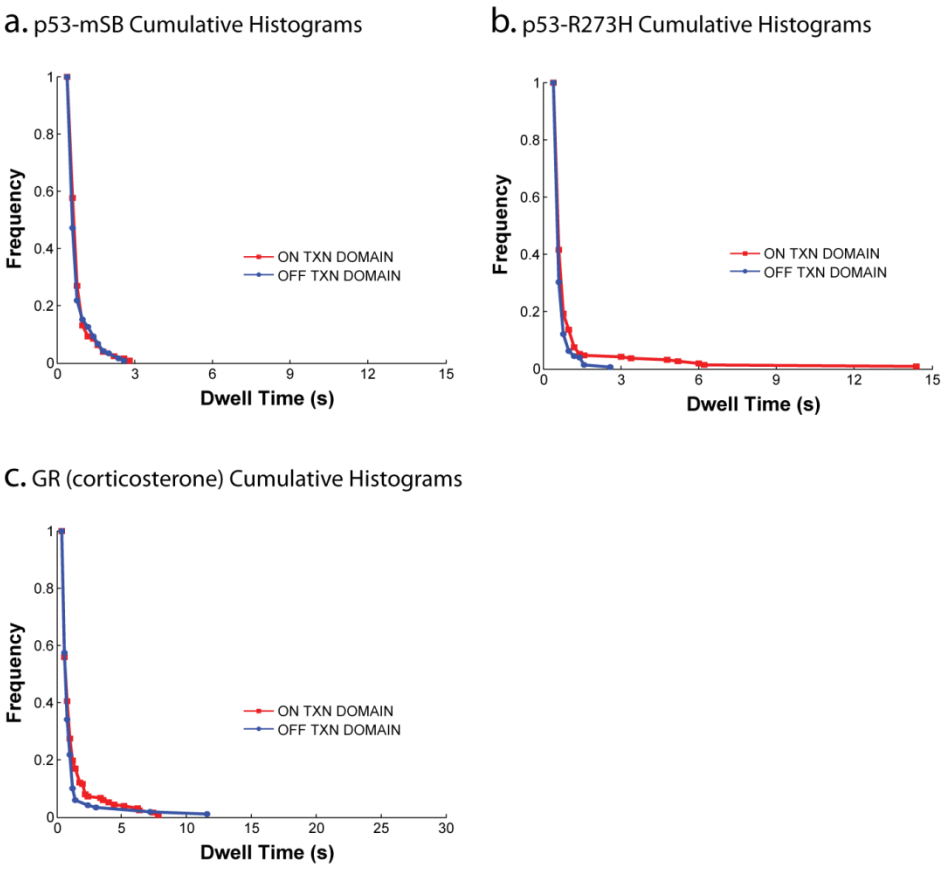

Supplementary Figure 6: Cumulative histograms of p53-mSB (a), p53-R273H (b) and GR stimulated with corticosterone (c) within and outside of transcription domains. Note that only p53-mSB showed a comparable distribution of dwell times within and outside of transcription domains.

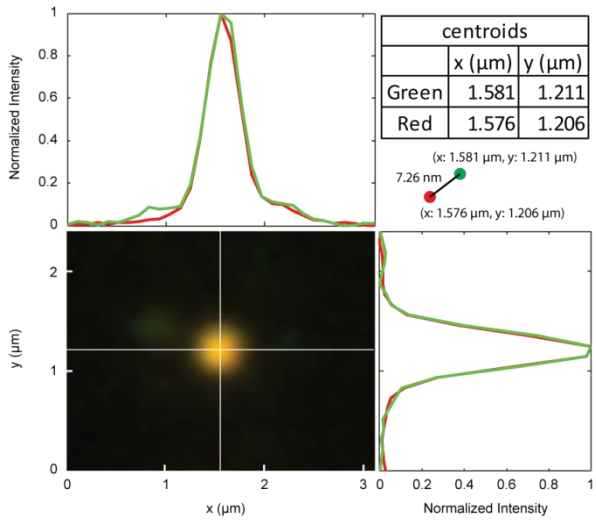

Supplementary Figure 7: Chromatic aberration test. We imaged a slide containing multicolor beads (TetraSpeck Microspheres, Molecular Probes) under the same imaging conditions used to visualize GFP polymerase II and TMR-HaloTag-TFs. We fit the acquired bead images with Gaussians along x and y profiles through the center of the bead. The peaks of these Gaussian fits in the red and green channels yielded the (x,y) coordinates for the centroid of the red and green images. For the particular bead shown here, the red and green centroids differed by 7.3 nm. A similar measurement for three other beads led to an average distance between red and green centroids of 10.5 ± 6.2 nm (n=5, average ± s.d.), which is less than the estimated spatial precision of 27 nm of our single molecule microscope[3]. This demonstrates that chromatic aberration is not a problem in our experiments.

Supplementary Table 1

first point (sec)	Probability of a free molecule (1 MDa) remaining in place	dwell times (sec) and slow fractions (%)									
		p53				p53-mSB		p53-R273H			
		OFF	ON TXN domain			OFF	ON	OFF	ON TXN domain		
		1-comp	Fast	Slow	Fraction	1-comp	1-comp	1-comp	Fast	Slow	Fraction
0.2	n.a.	0.15 ± 0.02	0.14 ± 0.01	1.3 ± 0.35	3.8 ± 0.9	0.20 ± 0.02	0.21 ± 0.03	0.15 ± 0.01	0.12 ± 0.02	0.49 ± 0.25	6.2 ± 5.4
0.4	1.8×10^{-2}	0.24 ± 0.03	0.22 ± 0.03	2.5 ± 0.75	4.2 ± 1.0	0.30 ± 0.05	0.33 ± 0.04	0.18 ± 0.03	0.21 ± 0.02	4.9 ± 3.0	1.1 ± 0.35
0.6	3.2×10^{-4}	0.28 ± 0.07	0.39 ± 0.06	4.2 ± 1.4	6.0 ± 1.4	0.43 ± 0.11	0.31 ± 0.07	0.27 ± 0.07	0.23 ± 0.05	6.0 ± 5.1	1.3 ± 0.50
0.8	5.8×10^{-6}	0.45 ± 0.07	0.47 ± 0.10	4.9 ± 2.1	7.0 ± 2.0	0.66 ± 0.06	0.47 ± 0.14	0.42 ± 0.15	0.29 ± 0.13	7.8 ± 9.8	2.1 ± 1.6
1.0	1.0×10^{-7}	0.47 ± 0.13	0.45 ± 0.16	4.8 ± 2.3	6.7 ± 3.0	0.67 ± 0.10	0.73 ± 0.13	0.55 ± 0.39	0.15 ± 0.08	5.8 ± 2.6	0.08 ± 0.27
average	n.a.	0.32 ± 0.14	0.33 ± 0.15	3.5 ± 1.6	5.5 ± 1.5	0.45 ± 0.21	0.41 ± 0.20	0.31 ± 0.17	0.20 ± 0.07	5.0 ± 2.7	2.1 ± 2.4

Supplementary Table 1: Fitting parameters obtained for the dwell time histograms of wild type p53, p53-mSB and p53-R273H, the p53 site-specific DNA binding mutants. For the histograms OFF transcription domains and the histogram of p53-mSB ON transcription domains, one component fits were satisfactory and so here the dwell time for that 1 component fit (1-comp) is shown. For the histograms ON transcription domains (except for p53-mSB), two component fits were necessary, and so here the dwell times for the fast and slow components are reported along with the size of the slow fraction. The first column shows the starting time point for the fit. Note that dwell times increase as fewer starting time points are included. The second column shows the probability that a 1 MDa molecular weight TF complex undergoing simple (non-anomalous) diffusion might be inadvertently included in the dwell time distribution. The final row shows the average values obtained from the fits starting at the different first time points. These average values are reported in the main text.

Supplementary Table 2

first point (sec)	Probability of a free molecule (1 MDa) remaining in place	dwell times (sec) and slow fractions (%)										
		GR (dexamethasone)							GR (corticosterone)			
		OFF	ON TXN domain			at array			OFF	ON TXN domain		
		1-comp	Fast	Slow	Fraction	Fast	Slow	Fraction	1-comp	Fast	Slow	Fraction
0.2	n.a.	0.14 ± 0.02	0.17 ± 0.01	4.9 ± 1.4	3.4 ± 0.50	0.39 ± 0.07	5.4 ± 0.49	38 ± 3.0	0.21 ± 0.04	0.14 ± 0.02	1.1 ± 0.29	6.8 ± 1.6
0.4	1.8×10^{-2}	0.29 ± 0.07	0.27 ± 0.03	7.3 ± 1.9	5.6 ± 0.94	0.60 ± 0.16	5.8 ± 0.61	45 ± 4.4	0.37 ± 0.03	0.31 ± 0.04	2.8 ± 0.92	6.9 ± 1.8
0.6	3.2×10^{-4}	0.49 ± 0.06	0.44 ± 0.05	9.6 ± 1.4	11 ± 1.3	0.63 ± 0.24	5.9 ± 0.67	47 ± 7.6	0.38 ± 0.07	0.42 ± 0.06	3.6 ± 1.2	7.6 ± 1.9
0.8	5.8×10^{-6}	0.44 ± 0.08	0.39 ± 0.06	9.2 ± 1.2	8.8 ± 2.2	0.56 ± 0.29	5.8 ± 0.66	42 ± 15.5	0.37 ± 0.13	0.34 ± 0.08	3.3 ± 0.87	6.0 ± 2.0
1.0	1.0×10^{-7}	0.50 ± 0.17	0.43 ± 0.11	9.5 ± 1.3	11 ± 5.7	0.37 ± 0.22	5.7 ± 0.52	21 ± 25	0.30 ± 0.22	0.42 ± 0.19	3.5 ± 1.3	8.6 ± 5.4
average	n.a.	0.37 ± 0.16	0.34 ± 0.12	8.1 ± 2.1	8.0 ± 3.5	0.51 ± 0.12	5.7 ± 0.20	39 ± 11	0.33 ± 0.07	0.32 ± 0.11	2.8 ± 1.0	7.2 ± 1.0

Supplementary Table 2: Fitting parameters obtained for the dwell time histograms of GR OFF and ON transcription domains throughout the nucleus (in the presence of dexamethasone or corticosterone), and ON transcription domains at the MMTV array (in the presence of dexamethasone). Table structure is the same as Table S1 except that there is no OFF transcription domain at the MMTV array, as the entire array shows high levels of polymerase II accumulation.

Supplementary Note 1: Testing robustness of the fitting procedure

In single molecule tracking, short dwell times reflect a mix of weak binding and episodes of slow diffusion, so diffusion will contaminate some fraction of the short dwell time events. Although different approaches have been devised to distinguish between diffusion and short binding events[2–4], it is difficult to completely eliminate contaminating diffusion events when attempting to estimate the shortest residence times on chromatin. Here, rather than applying a particular criterion, we fit the dwell time distributions varying the number of early time points included in the distribution. Specifically, we fit the data excluding either 0, 1, 2, 3 or 4 of the first time points, corresponding at our frame rates to 0.2, 0.4, 0.6, 0.8 and 1 s minimum dwell times. As more early time points are excluded the probability that the measurements reflect purely binding increases, but at the cost of omitting some of the shorter chromatin residence times.

Regardless of how many early time points we omitted, we found that our histogram data could be well fit with exponential decay models (Fig. S5). We also found as expected that as we omitted progressively more early points in the fit, the predicted residence times from the fits increased (Tables S1,S2). However, we consistently found the two residence times predicted from the two component fits were about an order of magnitude different (Tables S1,S2). Furthermore, we consistently found that the single component dwell time away from transcription domains was comparable to the fast component dwell time within transcription domains (Tables S1,S2). Thus while the absolute dwell times changed somewhat as more early time points were omitted from the fits, the overall conclusions obtained from the fits were unaffected.

SUPPLEMENTARY REFERENCES

1. Schneider, G. *et al.* Three-dimensional cellular ultrastructure resolved by X-ray microscopy. *Nat. Methods* **7,** 985–987 (2010).
2. Speil, J. *et al.* Activated STAT1 transcription factors conduct distinct saltatory movements in the cell nucleus. *Biophys. J.* **101,** 2592–2600 (2011).
3. Mazza, D., Abernathy, A., Golob, N., Morisaki, T. & McNally, J. G. A benchmark for chromatin binding measurements in live cells. *Nucleic Acids Res.* **40,** e119 (2012).
4. Persson, F., Lindén, M., Unoson, C. & Elf, J. Extracting intracellular diffusive states and transition rates from single-molecule tracking data. *Nat. Methods* **10,** 265–269 (2013).